Effects of Inelastic Neutrino-Nucleus Scattering on Supernova Dynamics and Radiated Neutrino Spectra

K. Langanke,[1,2] G. Martínez-Pinedo,[1] B. Müller,[3] H.-Th. Janka,[3] A. Marek,[3] W. R. Hix,[4] A. Juodagalvis,[5] and J. M. Sampaio[6]

[1]*Gesellschaft für Schwerionenforschung Darmstadt, Planckstrasse 1, D-64259 Darmstadt, Germany*
[2]*Institut für Kernphysik, TU Darmstadt, Schlossgartenstrasse 9, D-64289 Darmstadt, Germany*
[3]*Max-Planck-Institut für Astrophysik, Karl-Schwarzschild-Strasse 1, D-85741 Garching, Germany*
[4]*Physics Division, Oak Ridge National Laboratory, Oak Ridge, Tennessee 37831, USA*
[5]*Institute of Theoretical Physics and Astronomy, A. Gostauto 12, 01108 Vilnius, Lithuania*
[6]*Centro de Física Nuclear da Universidade de Lisboa, Avenida Professor Gama Pinto 2, P-1649-003 Lisboa, Portugal*

(Received 12 June 2007; published 3 January 2008)

Based on the shell model for Gamow-Teller and the random phase approximation for forbidden transitions, we calculate cross sections for inelastic neutrino-nucleus scattering (INNS) under supernova (SN) conditions, assuming a matter composition given by nuclear statistical equilibrium. The cross sections are incorporated into state-of-the-art stellar core-collapse simulations with detailed energy-dependent neutrino transport. While no significant effect on the SN dynamics is observed, INNS increases the neutrino opacities noticeably and strongly reduces the high-energy tail of the neutrino spectrum emitted in the neutrino burst at shock breakout. Relatedly the expected event rates for the observation of such neutrinos by earthbound detectors are reduced by up to about 60%.

DOI: 10.1103/PhysRevLett.100.011101 PACS numbers: 97.60.Bw, 25.30.Pt, 26.50.+x, 95.55.Vj

The simulation of core-collapse supernovae (SNe) is one of the great astrophysical challenges requiring sophisticated computational skills and detailed input from various fields of physics (e.g., [1,2]). It is well known that processes mediated by the weak interaction play an essential role for the collapse dynamics and the explosion mechanism [3–5]. However, inelastic neutral-current neutrino scattering on nuclei (INNS), $A + \nu \rightarrow A^\star + \nu'$, where A, $A^\star$ describe the nucleus with mass number A before and after the scattering process, has not yet been satisfactorily considered in SN simulations. In this process, energy is exchanged between neutrinos and matter, and hence it can potentially contribute to SN physics by (i) speeding up the thermalization of neutrinos with matter after neutrino trapping during the collapse phase, (ii) changing the neutrino opacity which will in turn modify the spectra of neutrinos released in the SN and to be observed by earthbound detectors, (iii) preheating the matter outside the shock front after bounce before arrival of the shock [6], (iv) reviving the stalled shock, and (v) spallating nucleons from nuclei and thus modifying explosive nucleosynthesis. In this Letter we will report about SN simulations which consider INNS reactions and allow us to explore topics (i)–(iii) in detail.

The effect of INNS in SN simulations has been investigated previously in an exploratory study [7], approximating the matter composition by a representative nucleus, ^{56}Fe. The reaction cross sections were based on a nuclear model for temperature $T = 0$, combining a truncated shell model evaluation of the allowed Gamow-Teller (GT) response to the cross section with estimates of forbidden components derived from the Goldhaber-Teller model. The study concluded that INNS rates can compete with those of neutrino-electron scattering at moderate and high neutrino energies ($E > 25$ MeV), while they are significantly smaller for low E. No significant effects of INNS on the stalled shock by preheating the accreted matter were found in [7].

Approximating the composition of SN matter by the ground state of the even-even nucleus ^{56}Fe is too simple an assumption for the calculation of INNS cross sections. Up to moderate neutrino energies, this neutral-current process is dominated by GT transitions mediated by the operator $\mathrm{GT}_0 = \boldsymbol{\sigma}\boldsymbol{\tau}_0$, where $\boldsymbol{\tau}_\pm$, $\boldsymbol{\tau}_0$ are the components of the isospin operator in spherical coordinates. The spin operator $\boldsymbol{\sigma}$ can only connect the ^{56}Fe ground state with spin and parity $J_i = 0^+$ to final states in the same nucleus with $J_f = 1^+$. As the lowest 1^+ state in ^{56}Fe is at an excitation energy of $E_x = 3$ MeV, there exists a threshold for inelastic neutrino scattering on ^{56}Fe (similarly on other even-even nuclei) and the cross sections are rather small for low neutrino energies.

Supernova matter consists of a mixture of many nuclei with even and odd proton and neutron numbers. Since odd-A and odd-odd (i.e., with odd proton and neutron numbers) nuclei miss the strong pairing gap that lowers the ground state in even-even nuclei relative to excited states, and have usually $J_i \neq 0$, GT transitions from the ground state to levels at rather low excitation energies are possible, reducing the threshold for inelastic neutrino scattering on the ground state and generally increasing the cross sections at low E. More importantly, SN matter has a nonzero temperature of order 1 MeV or higher, requiring the description of nuclei as a thermal ensemble [8]. This

completely removes the energy threshold for inelastic neutrino scattering, because nuclei are with nonvanishing probability in excited states that can be connected to the ground state or final states at smaller excitation energies. Such scattering events correspond to deexcitation of the nucleus with the consequence that the final neutrino energy E' is larger than the initial energy E, and can drastically increase the INNS cross sections for low neutrino energies at $T > 0$ [9].

Since the temperature is sufficiently high ($T \gtrsim 1$ MeV) once the inelastic process becomes relevant, the nuclear composition is well approximated by nuclear statistical equilibrium (NSE). The relevant INNS cross section $d\sigma(E, E')/dE'$ is obtained by folding the cross sections $d\sigma_i(E, E')/dE'$ for individual nuclei with the appropriate abundance distributions, $d\sigma(E, E')/dE' = \sum_i Y_i d\sigma_i(E, E')/dE' = (\sum_i Y_i)\langle d\sigma(E, E')/dE'\rangle$, where the sum runs over all nuclei present and Y_i denotes the number abundance n_i/n_b of a given species (n_i and n_b being the number densities of nuclei and baryons, respectively). Like in [4], we have calculated the abundances Y_i from a Saha-like NSE distribution, including Coulomb corrections [10,11] and the thermal population of excited states (using the partition function data of [12]).

The computation of cross sections for individual nuclei was described in [13], where the allowed GT transitions for inelastic neutrino scattering on the ground states were calculated within the shell model. Because of the absence of experimental data for INNS this approach was validated by detailed comparison to precision $M1$ data from inelastic electron scattering, which for spherical nuclei is dominated by transitions mediated by an operator proportional to GT_0 [14]. The contributions from forbidden transitions, which become increasingly important at moderate and high E, were evaluated within the random phase approximation (RPA). To incorporate the $T \neq 0$ effects, our treatment distinguishes between "up-scattering" (i.e., the final neutrino energy is smaller than the initial one; $E' < E$) and "down-scattering" ($E' > E$) contributions to the cross sections. Up-scattering was treated approximately assuming the Brink hypothesis, i.e., assuming that the GT_0 and forbidden distributions on the excited states are the same as calculated for the ground state. The down-scattering contribution is obtained from the up-scattering contribution using detailed balance from the thermally populated states.

Reference [13] has presented detailed cross sections for inelastic neutrino scattering on 40 nuclei of the $Z = 25$–28 isotope chains. Additionally, using the method described above we have also included 10 cross sections for the Cr ($Z = 24$) isotopic chain. Importantly, for $T \gtrsim 1$ MeV, all these calculations show little variations between individual cross sections. Therefore, we have assumed that the average cross section over the full composition can be approximated by $\langle d\sigma(E, E')/dE'\rangle \approx \sum_i' Y_i d\sigma_i(E, E')/dE'/\sum_i' Y_i$, where the sum is restricted to the pool of nuclei for which individual cross sections have been calculated. We have determined a cross section table for a large variety of temperatures ($0.517 \leq T[\mathrm{MeV}] \leq 3.447$), densities ($10^8 \leq \rho[\mathrm{g\,cm^{-3}}] \leq 6.31 \times 10^{12}$), and density dependent electron-to-baryon ratios ($0.23 \leq Y_e \leq 0.55$), for a mesh of initial and final neutrino energies between zero and 100 MeV.

Figure 1 shows the normalized final-energy neutrino spectra for three different initial energies. For $E \lesssim 10$ MeV down-scattering contributes significantly to the cross section; i.e., the deexcitation of thermally populated nuclear levels produces neutrinos with $E' > 10$ MeV. Down-scattering becomes essentially irrelevant at higher neutrino energies. For $E = 30$ MeV the cross section is dominated by the excitation of the GT_0 centroid, giving rise to a cross section peak around $E' = 20$ MeV. For even higher neutrino energies forbidden transitions contribute noticeably to the cross section. The peaks for $E = 50$ MeV correspond to excitations of the centroids of the GT_0 and dipole transition strengths.

The SN calculations presented in this work were performed in spherical symmetry with the neutrino-hydrodynamics code VERTEX (for details, see [15,16]). The code module that integrates the nonrelativistic hydrodynamics equations is a conservative, Eulerian implementation of a Godunov-type scheme with higher-order spatial and temporal accuracy. The self-gravity of the stellar gas is treated with an approximation to general relativity as discussed in [17] and tested against fully relativistic simulations in [17,18]. The time-implicit transport routine solves the moment equations for neutrino number, energy, and momentum. It employs a variable Eddington closure factor that is obtained from iterating to convergence a simplified Boltzmann equation coupled to the set of its moment equations. A state-of-the-art description of the interactions of neutrinos (ν) and antineutrinos ($\bar{\nu}$) of all flavors is included according to [16,19,20].

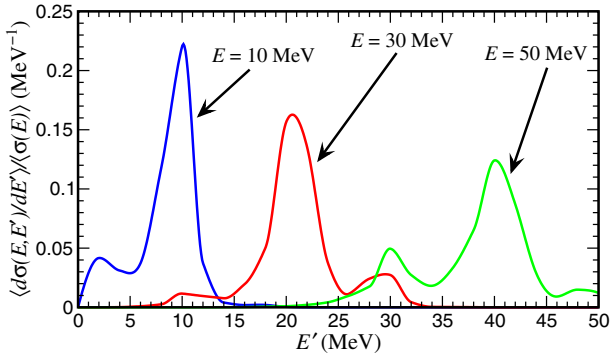

FIG. 1 (color online). Normalized final-energy neutrino spectra for initial neutrino energies of 10, 30, and 50 MeV and $T = 1$ MeV, $\rho = 6 \times 10^{11}$ g cm^{-3}, and $Y_e = 0.397$. The total composition averaged cross section, $\langle\sigma(E)\rangle$ (in units of 10^{-42} cm^2), for these energies is 0.48, 38, 243, respectively, and 0.97, 41, 267 for $T = 2$ MeV, $\rho = 2.5 \times 10^{12}$ g cm^{-3}, and $Y_e = 0.275$, and the same energies, showing a slight dependence on conditions.

We compare here the effects of INNS by simulating the collapse of a $15M_\odot$ progenitor star (model s15a28 of [21]) with three different nuclear equations of state (EOSs) from Lattimer & Swesty (LS) [22], Shen *et al.* [23], and Hillebrandt & Wolff [24], which are applied above some minimum density ($\sim 10^8$ g cm^{-3} before shock breakout and 10^{11} g cm^{-3} afterwards). At lower densities a mixture of ideal gases of $e^{\pm}$, photons, nucleons, and nuclei is used, and changes in the chemical composition are determined by temperature dependent stages or a 17-species NSE network, where appropriate. The high-density EOSs yield different time-variable abundances of neutrons, protons, α-particles, and a representative heavy nucleus, whose charge and mass numbers (Z, A) also differ between the three considered cases. As a consequence, the INNS cross sections for ν and $\bar{\nu}$ of all flavors are computed as the product of the tabulated pool-averaged differential cross sections, $\langle d\sigma(E, E')/dE' \rangle$, and an EOS-dependent abundance Y_A of the representative heavy nucleus. To reduce the dimensionality of the table, information of the cross section variation with the scattering angle was not stored. In the hydrodynamic simulations we therefore made the approximation that neutrinos colliding inelastically with nuclei are redistributed isotropically.

The effects of INNS on the SN evolution and the properties of the emitted neutrinos turn out to be very similar for all three employed nuclear EOSs. Despite causing a higher neutrino opacity by additional neutrino-nucleus interactions, INNS leads to a slightly stronger deleptonization and to a very small increase of the entropy in the homologously collapsing inner core, both less than 1%. These effects are caused by up-scattering reactions in which high-energy neutrinos from electron captures lose part of their energy, thus producing additional heating of the stellar matter and escaping faster from the stellar interior because neutrinos with lower energies possess a much smaller total interaction probability. The weak additional deleptonization reduces the collapse time to bounce and the enclosed mass of the shock formation radius minimally. Because of the additional opacity, the number of electron neutrinos radiated in the luminous burst that is released when the shock breaks out from the neutrino-opaque to the neutrino-transparent regime, is slightly smaller (on the third digit) when INNS is included. However, these reactions increase the neutrino-matter coupling and thus the total energy transfer rate (mainly on electrons and nuclei) ahead of the shock by typically a factor of 2–3 during the first $\lesssim 50$ ms after core bounce (before the shock reaches a radius where the preshock density drops below the minimum value of our cross section table so that INNS was not taken into account any longer). Nevertheless, these larger preshock heating rates act for too short a time on this supersonically infalling matter to lead to consequences for the shock propagation and SN dynamics. The differences with and without INNS remain smaller than the numerical resolution limit during all the simulated post-bounce evolution.

The most significant impact of INNS on the radiated neutrino spectra occurs in a time interval of about 15 ms around the shock breakout ν_e burst, when the preshock matter, which is composed mainly of heavy nuclei in NSE, has still a high density and therefore a fairly large optical depth for the escaping neutrinos. For this reason, high-energy neutrinos are efficiently degraded in energy space by frequent inelastic collisions with nuclei. While the mean spectral energy is reduced only by a modest amount (0.4–0.5 MeV), the high-energy tail of the emitted ν_e burst spectrum is strongly suppressed. The normalized spectra of electron neutrinos during a time interval of 8 ms around the maximum luminosity of the burst for simulations with and without INNS are displayed in Fig. 2. A similar effect of INNS is observed for $\bar{\nu}_e$ and heavy-lepton neutrinos ν_x (see [1]) when their luminosities begin to rise at the time the ν_e emission comes down from its peak but still remains clearly dominant for some ten milliseconds.

Considering that the neutrino absorption cross sections on nuclei typically increase steeply with E, the reduction of the high-energy spectral tail has consequences for the detectability of the ν_e burst from SNe by experiments (see, e.g., [25–27]). This is demonstrated in Table I, where we compare the relevant ν_e detection cross sections calculated for the SN spectrum with and without INNS. The largest reduction occurs for ^{12}C (35%) and ^{16}O (60%), which are detector materials in Borexino, MiniBooNe, KamLAND, SNO +, and Super-Kamiokande, as only neutrinos with relatively high energies ($E > 17$ MeV for ^{12}C and 15 MeV for ^{16}O) can trigger charged-current reactions. The data for ^{12}C (N_{gs}) include only the transition to the ^{12}N ground state. This is the only bound state in ^{12}N and the easiest transition to detect, because ^{12}N decays by e^+ emission after 11 ms. We find a reduction of 11% for the (ν_e, e^-) cross section on ^{40}Ar (the detector material in ICARUS), 17% for ^{56}Fe (Minos), and ^{208}Pb (OMNIS). In

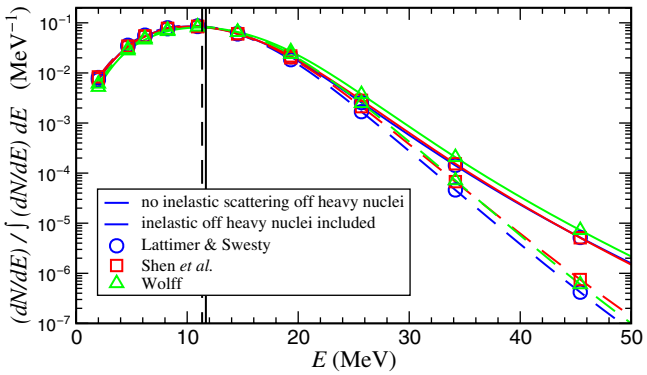

FIG. 2 (color online). Normalized ν_e number spectra radiated during the shock breakout burst as seen by a distant observer at rest obtained with three different nuclear EOSs. The vertical lines mark the mean spectral energies (for the Lattimer & Swesty EOS, $\langle E \rangle = 11.68$, 11.34 MeV without and with INNS; the second moments are $\langle E^2 \rangle = 159.3$, 149.3 MeV^2). The symbols mark the location of the energy grid points.

TABLE I. Electron neutrino cross sections for scattering off electrons and for charged-current interactions with nuclei of different detector materials, averaged over the SN spectrum of Fig. 2, using the results obtained with the L&S EOS (the Wolff EOS gives similar results, while the Shen *et al.* EOS predicts a slightly smaller reduction). The different cross sections are taken from: e [28] (with a 5 MeV threshold for the electron energy), ^{12}C [29], ^{16}O [30], ^{40}Ar [31], ^{56}Fe, and ^{208}Pb [32].

Material	$\langle\sigma\rangle$ (10^{-42} cm^2)		Reduction
	With INNS	Without INNS	
e	0.058	0.061	5%
^{12}C	0.050	0.080	37%
^{12}C (N_{gs})	0.046	0.071	35%
^{16}O	0.0053	0.0128	58%
^{40}Ar	13.4	15.1	11%
^{56}Fe	6.2	7.5	17%
^{208}Pb	103.3	124.5	17%

contrast, since the cross section for scattering off electrons increases linearly with E, its reduction is relatively small (only 5%), which is relevant for Super-Kamiokande. Using the LS EOS, 1.5×10^{56} ν_e are emitted in total during the shock breakout burst. For a SN at 10 kpc distance, INNS leads to a reduction from 8.3 to 7.7 charged-current events for Super-Kamiokande (32 ktons water), from 9.2 to 8.2 for ICARUS (3 ktons Liquid Argon) [33], from 13.6 to 11.3 for OMNIS (3 ktons lead) [34], and from 2.2 to 1.4 for LENA (50 ktons C_nH_{2n}) [35].

In summary, we have reported on SN simulations which greatly improve the treatment of INNS, which allows for an additional mode of energy exchange between neutrinos and matter. We found that this mode has little effect on the collapse dynamics and the shock propagation. However, INNS modifies the radiated neutrino spectra. In particular, INNS strongly reduces the high-energy spectral tail of the ν_e burst at shock breakout. In turn, this noticeably decreases the cross section for the observation of the burst neutrinos from future SNe by neutrino detectors.

In Garching, this work was supported by DFG Grants No. SFB/TR 27 and No. SFB 375 and by the cluster of excellence Origin and Structure of the Universe. J. M. S. acknowledges a grant from Fundação para a Ciência e Tecnologia. Oak Ridge National Laboratory is managed by UT-Battelle, LLC, for the US Department of Energy under Contract No. DE-AC05-00OR22725.

[1] H.-T. Janka, K. Langanke, A. Marek, G. Martínez-Pinedo, and B. Müller, Phys. Rep. **442**, 38 (2007).
[2] A. Mezzacappa, Annu. Rev. Nucl. Part. Sci. **55**, 467 (2005).
[3] H. A. Bethe, Rev. Mod. Phys. **62**, 801 (1990).
[4] K. Langanke and G. Martínez-Pinedo, Rev. Mod. Phys. **75**, 819 (2003).
[5] A. Burrows, S. Reddy, and T. A. Thompson, Nucl. Phys. **A777**, 356 (2006).
[6] W. C. Haxton, Phys. Rev. Lett. **60**, 1999 (1988).
[7] S. W. Bruenn and W. C. Haxton, Astrophys. J. **376**, 678 (1991).
[8] G. M. Fuller and B. S. Meyer, Astrophys. J. **376**, 701 (1991).
[9] J. M. Sampaio, K. Langanke, G. Martínez-Pinedo, and D. J. Dean, Phys. Lett. B **529**, 19 (2002).
[10] W. R. Hix and F.-K. Thielemann, Astrophys. J. **460**, 869 (1996).
[11] E. Bravo and D. García-Senz, Mon. Not. R. Astron. Soc. **307**, 984 (1999).
[12] T. Rauscher, Astrophys. J. Suppl. Ser. **147**, 403 (2003).
[13] A. Juodagalvis, K. Langanke, G. Martínez-Pinedo, W. R. Hix, D. J. Dean, and J. M. Sampaio, Nucl. Phys. **A747**, 87 (2005).
[14] K. Langanke, G. Martínez-Pinedo, P. von Neumann-Cosel, and A. Richter, Phys. Rev. Lett. **93**, 202501 (2004).
[15] M. Rampp and H.-T. Janka, Astron. Astrophys. **396**, 361 (2002).
[16] R. Buras, M. Rampp, H.-T. Janka, and K. Kifonidis, Astron. Astrophys. **447**, 1049 (2006).
[17] A. Marek, H. Dimmelmeier, H.-T. Janka, E. Müller, and R. Buras, Astron. Astrophys. **445**, 273 (2006).
[18] M. Liebendörfer, M. Rampp, H.-T. Janka, and A. Mezzacappa, Astrophys. J. **620**, 840 (2005).
[19] K. Langanke, G. Martínez-Pinedo, J. M. Sampaio, D. J. Dean, W. R. Hix, O. E. B. Messer, A. Mezzacappa, M. Liebendörfer, H.-T. Janka, and M. Rampp, Phys. Rev. Lett. **90**, 241102 (2003).
[20] A. Marek, H.-T. Janka, R. Buras, M. Liebendörfer, and M. Rampp, Astron. Astrophys. **443**, 201 (2005).
[21] A. Heger, S. E. Woosley, G. Martínez-Pinedo, and K. Langanke, Astrophys. J. **560**, 307 (2001).
[22] J. M. Lattimer and F. D. Swesty, Nucl. Phys. **A535**, 331 (1991).
[23] H. Shen, H. Toki, K. Oyamatsu, and K. Sumiyoshi, Nucl. Phys. **A637**, 435 (1998).
[24] W. Hillebrandt, K. Nomoto, and R. G. Wolff, Astron. Astrophys. **133**, 175 (1984).
[25] K. Scholberg, arXiv:astro-ph/0701081.
[26] T. A. Thompson, A. Burrows, and P. A. Pinto, Astrophys. J. **592**, 434 (2003).
[27] M. Kachelrieß, R. Tomàs, R. Buras, H.-T. Janka, A. Marek, and M. Rampp, Phys. Rev. D **71**, 063003 (2005).
[28] G. 't Hooft, Phys. Lett. **37B**, 195 (1971).
[29] E. Kolbe, K. Langanke, and P. Vogel, Nucl. Phys. **A652**, 91 (1999).
[30] E. Kolbe, K. Langanke, and P. Vogel, Phys. Rev. D **66**, 013007 (2002).
[31] E. Kolbe, K. Langanke, G. Martínez-Pinedo, and P. Vogel, J. Phys. G **29**, 2569 (2003).
[32] E. Kolbe and K. Langanke, Phys. Rev. C **63**, 025802 (2001).
[33] A. Bueno, I. Gil-Botella, and A. Rubbia, arXiv:hep-ph/0307222.
[34] R. N. Boyd, A. S. J. Murphy, and R. L. Talaga, Nucl. Phys. **A718**, 222 (2003).
[35] L. Oberauer, F. von Feilitzsch, and W. Potzel, Nucl. Phys. B, Proc. Suppl. **138**, 108 (2005).